Scientific Challenges of UV-B Forecasting

Henning Staiger and Gudrun Laschewski

Deutscher Wetterdienst
Stefan-Meier-Str. 4, D-79104 Freiburg, Germany
Gudrun.Laschewski@dwd.de

1. Introduction

Overexposure to ultraviolet (UV) radiation from the sun is of considerable concern to public health and plays a major role in the development of skin cancer and eye damage (WHO 2003). A marked increase in the incidence of skin cancer has been observed in fair-skinned populations world-wide since the early 1970s (WHO 2002) and is estimated to about 130,000 new melanoma per year and to 66,000 death related to malignant melanoma. It has been projected that in 2005 in the United States will be more than 59,000 new cases of invasive melanoma, and 7,700 deaths related to melanoma, and that the cost of management of skin cancers will exceed US $ 800 million per year in the United States alone (Lim et al. 2005). The skin cancer incidence is in first priority associated with personal habits in relation to sun exposure and its ultraviolet component, and the societal view that a tan is desirable and healthy. Moreover, the risk of UV overexposure has increased as a consequence of the depletion of the ozone layer. Therefore, in 1992 the United Nations Conference on Environment and Development agreed under Agenda 21 “to undertake as a matter of urgency, research on the effects on human health of increasing UV reaching the earth surface as a consequence of depletion of the stratospheric ozone layer; and on the basis of the outcome of this research to consider taking appropriate remedial efforts to mitigate the effects on human beings”. In response to Agenda 21, WHO, in collaboration with WMO, IACR, and ICNIRP established INTERSUN, the Global UV Project (WHO 2003). One of four of INTERSUN’s priority activities is to facilitate the harmonisation of national activities on sun protection and the co-ordination of international activities through the use of the Global Solar *UV Index* and its associated health protection messages. The harmonised UV Index has been introduced collaboratively by WHO (2002), the ICNIRP (1995), the WMO (1995, 1998), and the UNEP to inform the public by means of an elementary physical quantity. Its main objective is to raise public awareness of the risk of excessive exposure to UV. It shall serve as educational tool to promote sun protection.

2. UV Index

The UV Index is a dimensionless value defined as the integrand between 280 and 400 nm of the spectral UV irradiance on a horizontal plane, W m^{-2} nm^{-1}, weighted with the CIE (1987) action spectrum on erythema (sunburn) induction in human skin and multiplied by the constant 40 W^{-1} m^2. The spectral erythemal effects (Fig. 1) have a maximum in the wavelength band 300 to 320 nm that is strongly associated with UV absorption by atmospheric ozone. The UV Index can be derived from physical measurements or radiative transfer calculations and can therefore be forecasted by using predictable meteorological parameters.

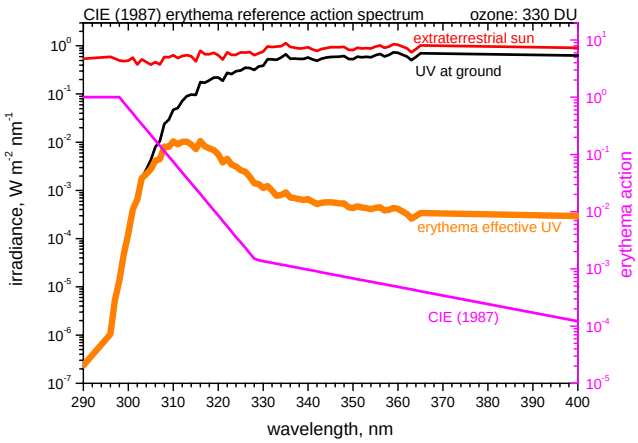

Figure 1 Spektral UV irradiance, CIE (1987) erythema action spectrum, and erythema effective UV

WMO (1998) recommends, that the UV Index shall account for cloud cover and further relevant environmental variables, and shall be reported to the public as the daily maximum *whenever it occurs.* Thus the UV Index is not a solar noon value alone.

In order to co-ordinate the activities for UV Index forecast in Europe and to improve the relevant scientific methodologies, COST Action 713 "UV-B-Forecasting" was undertaken (Bais 1999, Vanicek et al. 2000). Inter alia COST-713 recommended that forecasts of total column ozone should be produced by global dynamical models, that aerosol optical depth and aerosol absorption variable in space and season should be included, and that the UV Index calculation shall be based on multiple scattering algorithms.

The requirements related to ozone and aerosols associate UV Index forecasting with the scheduled results of the “Global Earth Monitoring System (GEMS)”.

3. Challenges of UV forecasting

Since 2002 dynamic forecasts of total column ozone are operational and near real time available in Europe from several sources, e.g. from KNMI (Eskes et al. 2002), ECMWF (Dethof and Hólm 2004a and b), MétéoFrance (Peuch et al. 2004), DWD (Majewski et al. 2002) initialised from ECMWF ozone analysis using algorithms resulting from the EU funded project STREAMER (Bittner and Erbertseder 2000). Available are several high quality multiple scattering models too. The challenges of UV forecasting are of operational nature, especially to account for higher resolution in time and the relevant environmental effects.

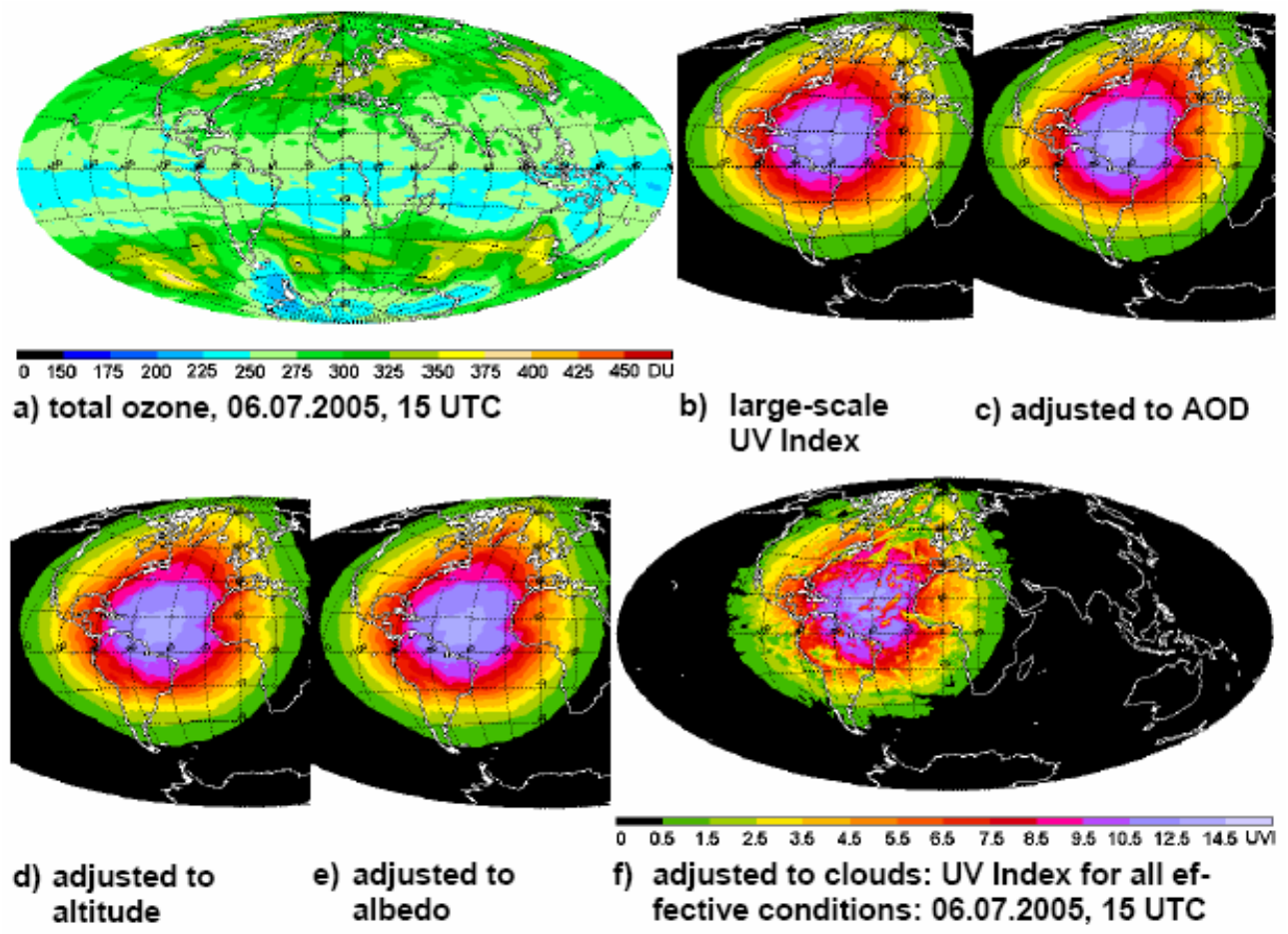

Figure 2 Modular structure of UV Index forecast by adjusting of the "large-scale UV Index"; valid July 06th, 2005, 00 UTC +15h: a) GSE PROMOTE forecast of total column ozone, b) large scale UV Index, c) adjustment to seasonal and regional varying aerosols, d) adjustment to altitude, e) adjustment to varying albedo of the surface, f) accounting for clouds.

Thus, UV-Index forecasting requires fast parameterisations to calculate the radiation transfer as accurate as possible and nevertheless accounting for all effective atmospheric conditions, namely aerosols, altitude effects, UV surface albedo, and clouds. DWD has implemented a method to forecast the UV-Index (UVI) having a modular structure (Staiger and Koepke 2005). It calculates a "large-scale UV Index" that is subsequently adjusted by factors to the UV Index for all effective atmospheric conditions:

$$\begin{aligned} UVI = {} & \text{large-scale\_UVI}(SZA, TOZ) \\ & * f_{aerosol}(AOD, SSA, SZA) \\ & * f_{altitude}(AOD, SSA, SZA, z) \\ & * f_{albedo}(ALB, SZA, z) \\ & \quad [\text{these steps of adjustment result in the UV Index clear sky}] \\ & * f_{clouds}(\text{cloud\_cover, cloud\_type[, SW-RAD]}) \end{aligned}$$

Fig. 2 demonstrates the modular structure of the UV Index calculation. The independent variables of the functions are solar zenith angle (SZA), total column ozone (TOZ), aerosol optical depth at 550 nm (AOD), single scattering albedo at 300 nm and 70 % relative humidity (SSA), the altitude above mean sea level (z), UV surface albedo (ALB), cloud cover and cloud types, and the short-wave global irradiance (SW-RAD).

4. Method

4.1. Radiation Transfer: Large-Scale UV Index

In general the UV irradiance decreases both with increasing SZA and increasing TOZ, both increase the number of absorbing ozone molecules along the path of the radiation through the atmosphere. The biologically active irradiances scale with larger ozone changes due to a power relationship (Madronich et al. 1998). The absolute effect of varying ozone amounts on the UV irradiation increases with the SZA and depends on aerosol properties and distribution (Schwander et al. 1997). However, the relative effect is practically independent of it (Koepke et al. 2002). Thus, the subsequent parameterisation of the aerosol and altitude effect on the UV Index can be made by means of a standardised total column ozone; DU 300 was selected.

Predictions of the UV Index for all hours and a global coverage become feasible using lookup tables (LUT). Uncertainties of UVI calculations under cloud- and snow-free conditions due to deviations from actual height profiles against monthly averages are < 3 % for ozone profiles, < 1 % for extinction profiles, < 2 % for temperature profiles (Schwander et al.1997, Reuder and Schwander 1999). According to the COST-713 recommendations a large-scale UV Index is produced as basic quantity that may be used for interpolation to the grid of high resolution models. The large scale UV Index is valid for mean sea level; clear sky conditions; albedo of the surface 3 %; aerosol types (Hess et al. 1998) "continental average" for 0 - 3 km, "free troposphere" for 3 - 12 km, and "stratosphere" above 12 km; and an aerosol optical depth at 550 nm of 0.20.

The LUT are prepared applying the high quality multiple scattering model STAR, System for Transfer of Atmospheric Radiation (Ruggaber et al. 1994), in the neural version STARneuro (Schwander et al. 2001). STAR is tested against models and measurements (Koepke et al. 1998; DeBacker et al. 2001, Mech and Koepke 2004). The LUT are calculated for the 15th of each month, and in each hemisphere for 5 zonal belts using monthly mean profiles of ozone taken from the UGAMP climatology (Li and Shine 1995), temperature and pressure profiles taken from "COSPAR International Reference Atmosphere" (Labitzke et al. 1985, Rees et al. 1990), and humidity profiles taken from the AFCLR data (McClatchey et al. 1972). The profiles are

interpolated to the standard profile of 33 homogenous layers recommended for STARneuro. Spectral UV irradiances and finally the UV Index are calculated as a function of SZA, resolution of 1°, and TOZ, resolution of 10 DU. The effective ozone forecasts are provided by the partner KNMI of the project GSE PROMOTE, and backed up by DWD's global model (GME) ozone forecasts. The UV Index is interpolated linearly in ozone, in the cosine of the SZA, and linearly for days between the 15th of two months, respectively.

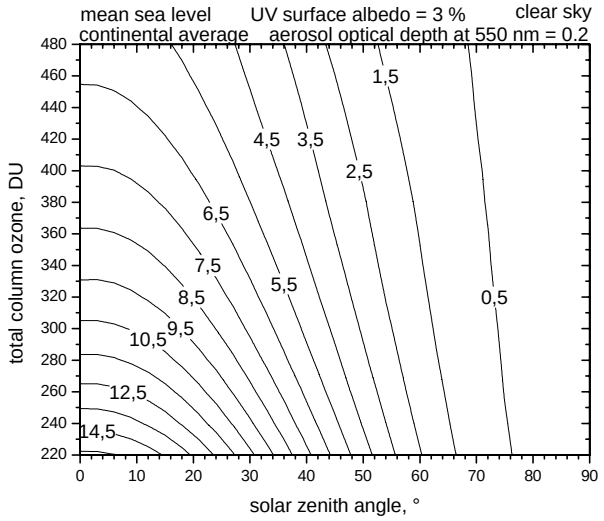

Figure 3Isolines of large-scale UV Index as function of solar zenith angle and total column ozone

Differences between radiation transfer by LUT and a complete calculation of the radiation transfer applying forecasted profiles of ozone and temperature are minimised by the monthly climatologies for 10 zonal belts. The deviations between the results of the lookup tables and a complete radiation transfer calculation applying forecasted profiles of ozone, temperature and pressure are less than 1.5 % in the majority of the cases. The standard deviation of the monthly averages is a half to one order lower than the average deviation.

The large-scale UV Index varies between zero, for sun beneath the horizon, and 12 to 15 for sun in the zenith and average TOZ of the tropics, Fig. 3.

4.2. Aerosol effects

Aerosol particles interact with solar radiation by scattering and absorption. UV irradiance at the Earth's surface decreases if the scattering and/or absorption properties of the atmospheric aerosols increases. The major aerosol effect on UV radiation results from differences in the aerosol optical depth and in the absorption properties. The aerosol type describes the spectrally dependent extinction coefficient, the absorption properties via the SSA, and the phase function (Hess et al. 1998, Koepke et al. 1997). The aerosol optical depth is the vertical integral of the extinction coefficients. The relative humidity causes a swelling of the aerosol particles and thus influences aerosol optical depth and SSA. For parameterisation it is set to 70 %. The relative aerosol profile type utilised is "volcanic background conditions", Fig. 4. It is scaled to the extinction profile according to the defined aerosol types (maritime clear, continental average, urban) and the given aerosol optical depth at 550 nm (AOD).

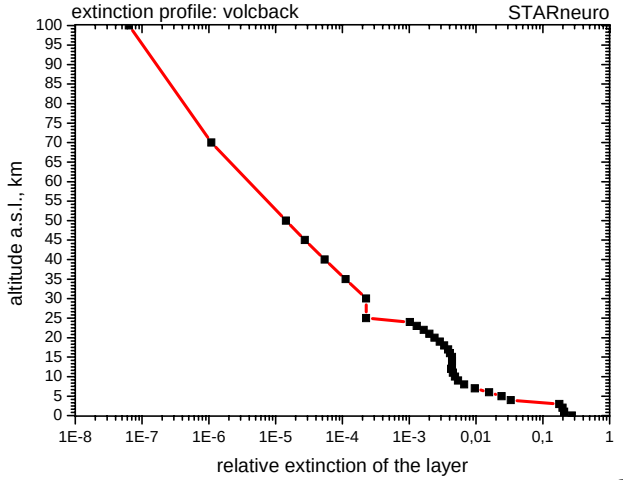

Figure 4 Vertical profile of the relative extinction

The SSA depends strongly on the aerosol type and less on the wavelength with the exception of the aerosol type "desert", Fig. 5. There are only small effects of a low AOD on the UV Index in dependence on the aerosol type (Fig. 6, dotted lines of all colours). In case of an almost non absorbing aerosol (maritime clear, mc, in Fig. 6) the decrease of UV irradiance stays small if the AOD increases (green broken and solid lines). This is due to the fact that on the one hand the direct beam will decrease strongly, otherwise the diffuse part of the irradiance will increase in the same order with the exception of photons scattered back to the space. Thus, the sum of the both components determining the UV Index will only slightly decrease. This does change significantly for aerosols with increasing absorption. Already for a moderately absorbing aerosol type e.g. "continental average" the seasonal cycle in AOD (e.g. 0.1 to 0.4 at 550 nm in Central Europe) can reduce the UV irradiance by up to 10 % (Fig. 6, broken black line), in case of a strong aerosol load (AOD 0.70) by more than 20 % (Fig. 6, solid black line). For a strong absorbing urban aerosol and a high AOD of 0.7 the reduction can exceed 35 % (Fig. 6, solid red line). In extreme cases aerosols can influence the UV Index up to an amount comparable to that of day to day changes in total ozone column (Jaroslawski and Krzyscin 2005).

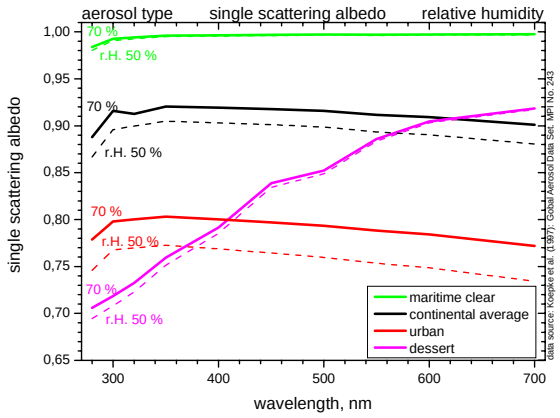

Figure 5 Single scattering albedo spectrally dependent on aerosol type and relative humidity

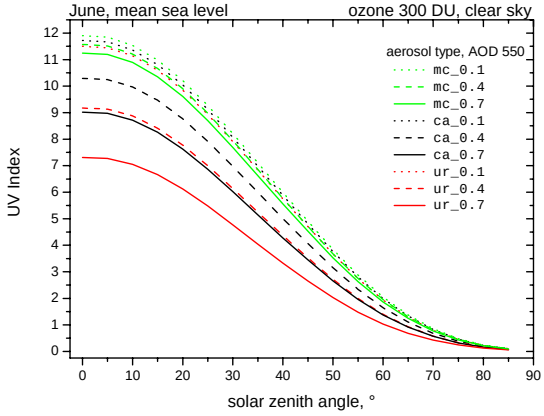

Figure 6 Index depending on aerosol type and aerosol optical depth at 550 nm: mc= maritime clear, ca = continental average, ur = urban

An adjustment of the large-scale UV Index to aerosol effects has to be made to spatially and temporally variable AOD and SSA. The conditions $UVI_{SSA:AOD}$ / $UVI_{ca:0.20}$ are almost linearly dependent on the logarithm of the AOD. The conversion factor from fixed to variable aerosols depends on AOD, SSA and SZA, Fig. 7. The dependence on SZA is relatively low and shows a maximum at a SZA of about 60°. For a continental average aerosol and an increase in AOD by 0.10 a rough estimation of the influence on the UV Index is a decrease of 3 to 4 %, for an urban aerosol the decrease in UV Index is about 4 to 5 %. The conversion of the set AOD of the large-scale UV Index to any AOD shows a maximum absolute error of 0.05 in the UV Index for the "continental average" aerosol type and 0.21 for "urban". Between the SSA's of the three aerosol types is linearly interpolated in the logarithm of the conversion factors. A comparison with the SSA of the aerosol type "continental clean", not used in parameterisation, reveals that the deviations show a minimum, if the SSA at 280 nm is applied. The maximal error for interpolation in SSA is < 0.27 UV Index in all cases of AOD and SZA.

Since forecasts of AOD and aerosol type are not yet available, regional monthly mean values of AOD have been derived from the monthly NASA MODIS "MOD08_M3" data 2000 to 2003 (Kaufman et al. 2002) and the 1979 to 2001 monthly means of aerosol optical depth at 550 nm derived from TOMS to fill the data gaps over the great deserts (Torres et al. 2002), see annex. The required SSA at 300 nm is taken from the "Global

Aerosol Data Set (GADS)"(Koepke et al. 1997) for a relative humidity of 70 %. On the basis of these large-scale structures the integration of the seasonal course of the AODs into the global forecast of the UV Index is realised. This has been taken into account in Fig. 2 c. Modifications of UV Index on a small scale, e.g. in regions with aerosol changed by urban influence, were not recorded. The parameterisations can, however, provide the basis for a particular adjustment of the "large-scale UV Index", if the specific conditions are known. For the future a significant improvement seems possible, if GEMS will provide such fields near real time assimilated and forecasted and with global coverage.

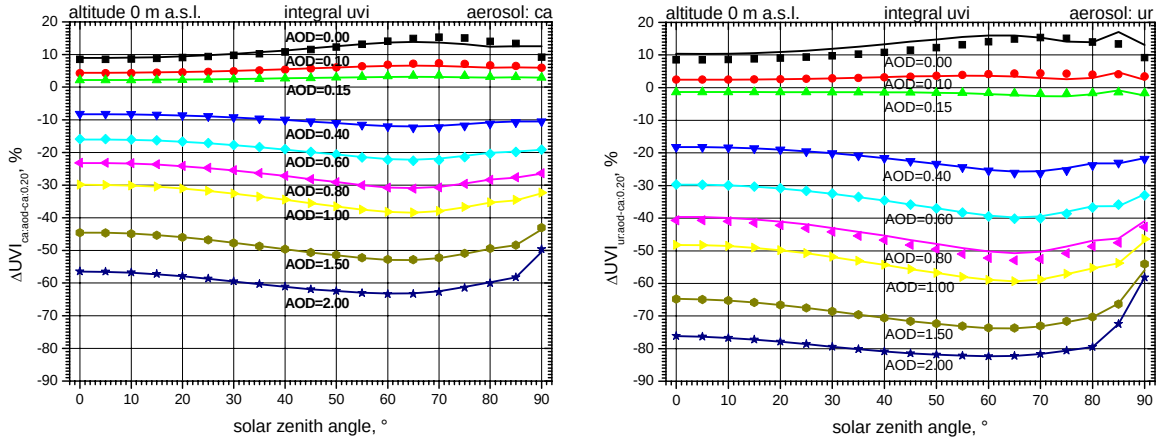

(a) ***(b)***

Figure 7 Effect of aerosol optical depth on the UV Index for(a) aerosol type „continental average" and (b) "urban" relative to an aerosol optical depth 0.20 for „continental average", 0 m MSL ($\Delta UVI_{ca:aod-ca:0.20}$). Symbols are modelled by STARneuro, lines are parameterised values

4.3. Altitude effect

With increasing altitude the UV Index generally increases (Blumthaler et al. 1993) due to the reduction of the attenuating material above the observer and the increasing radiation from below, resulting via multiple scattering from increasing albedo. The altitude effect (Schmucki and Philipona 2002) is defined as relative difference in the irradiance between two altitudes high and low, scaled to the uniform difference in altitude of 1 km. According to the suggestion by Pfeifer (2003), i.e. to give the altitude dependency separated as effects of different components, the ozone and the albedo influence are taken into account independently, and here the aerosol and altitude dependency is shown. It is approached analogue to the Bouguer-Lambert law by factors for aerosol and Rayleigh scattering. The Rayleigh scattering is the special case for AOD = 0. Its vertical distribution corresponds to that of the air pressure. The aerosol scattering and absorption is parameterised from STARneuro modelled values. The almost linear relationships to AOD that exist in the logarithm of the altitude dependency of the UV Index allow a parameterisation on the AOD without having to fear essential error sources. As the relationship is not completely linear, the fit is accomplished via the least squared deviations by means of a 2nd degree polynomial (Press et al. 1996). The parameterisation on the AOD dependency in altitude effect and on the adjustment of the fixed AOD of the large-scale UV Index to varying AOD has the advantage of greatly reducing the number of the required coefficients. The matrix of the coefficients for the altitude effect resulting from the parameterisation and the changes of the AOD at sea level are numerically efficient to be used for large numbers of calculations.

The mean profiles of ozone and temperature for the moderate latitudes in the northern hemisphere for the month of June are applied. The mixing layer altitude is fixed at 3 km above ground. It begins to shrink when its upper boundary has reached the maximal approved altitude of 5000 m above MSL. This corresponds more or less to the conditions in the Bolivian highlands (Pfeifer 2003). The radiation transfer calculations

were carried out for the three aerosol types “maritime clear”, “continental average” and “urban” in the mixing layer with known SSA (Hess et al 1998).

Figs. 8a and b show the altitude effect of the UV Index for the aerosol types “continental average“, and for “urban“, respectively, as function of SZA and for variable AOD. The effect of SZA is small, with a marginal maximum at SZA’s of between 60 and 70° for typical AOD’s that shifts to SZA of around 40 to 45° for higher AOD. The effects increase with increasing altitude difference. Generally the altitude effect is in the order of 10 % km^{-1} for an AOD of 0.4 (Fig. 8a) which however increases to about 14 % km^{-1} for the same AOD, but more strongly absorbing urban aerosol (Fig. 8b). This is in very good agreement with measured altitude effects of the UV Index (Piazena 1996, McKenzie et al. 2001, Pfeifer 2003).

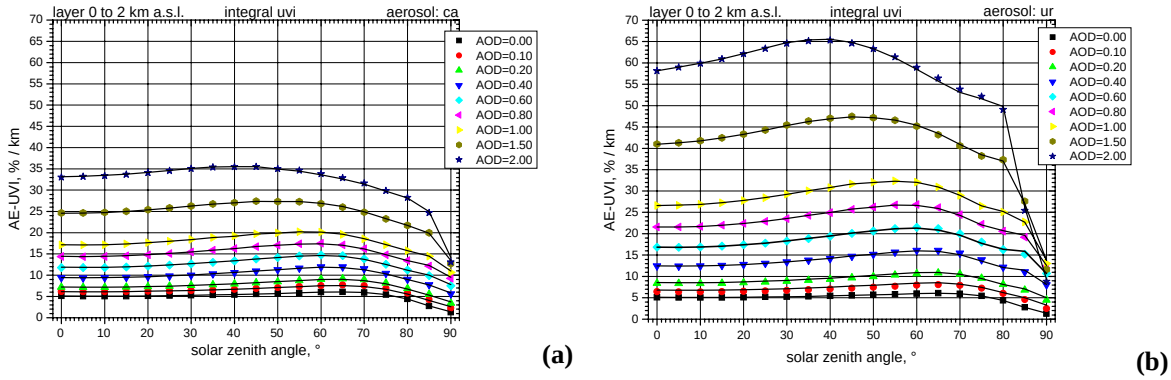

Figure 8 Altitude effect of UV Index dependent from solar zenith angle and aerosol optical depth, layer 0 to 2 km MSL, aerosol type (a) “continental average”, (b) „urban“. Symbols are modelled by STARneuro, lines are parameterised values.

In Fig. 2d in relation to Fig. 2c the altitude effect can be seen by the increase of the UV Index over the Andes and over Greenland. The uncertainties resulting from the parameterisation of the altitude effect has been determined quantitatively against the modelled values. The maximum error in the UV Index is 0.04 for the “continental average“ aerosol type, and for the type “urban”: 0.21, determined over all AOD’s, all altitude layers and all SZA’s.

4.4 Adjusting for snow albedo

Radiation reflected from the Earth’s surface contributes to UV irradiance by multiple scattering that redirect reflected photons towards the ground again. Strong variability of albedo in the seasonal cycle occurs only for areas where temporal snow cover is present, Fig. 9 (Tanskanen 2004). In the UV the albedo of the ground is markedly high only for snow and (sea-) ice (Feister and Grewe 1995). It may reach values higher than 0.9 for freshly fallen snow in Antarctica (Grenfell et al. 1994) where the terrain is homogeneously covered with snow. This assumption should also be valid for arctic regions and for the inland ice on Greenland. With these exceptions a terrain homogeneously covered with snow does not occur on a regional scale (Arola et al. 2003). Even during periods with snow cover trees, rocks, roads, roofs of buildings etc. often become snow free. Therefore the high albedo values measured by Grenfell et al. 1994, Feister and Grewe 1995, Blumthaler and Ambach 1988 are only rarely representative for the ground surface areas. Under natural conditions the irradiance at a receiver is affected by photons reflected by an area of up to 30 km^2. The irradiance enhancement compared to a completely absorbing ground shows values up to +40 % for an albedo of 80 %. For regional albedos lower than 10 % the enhancement is lower than 5 % and of minor importance, the set value of 3 % is unchanged.

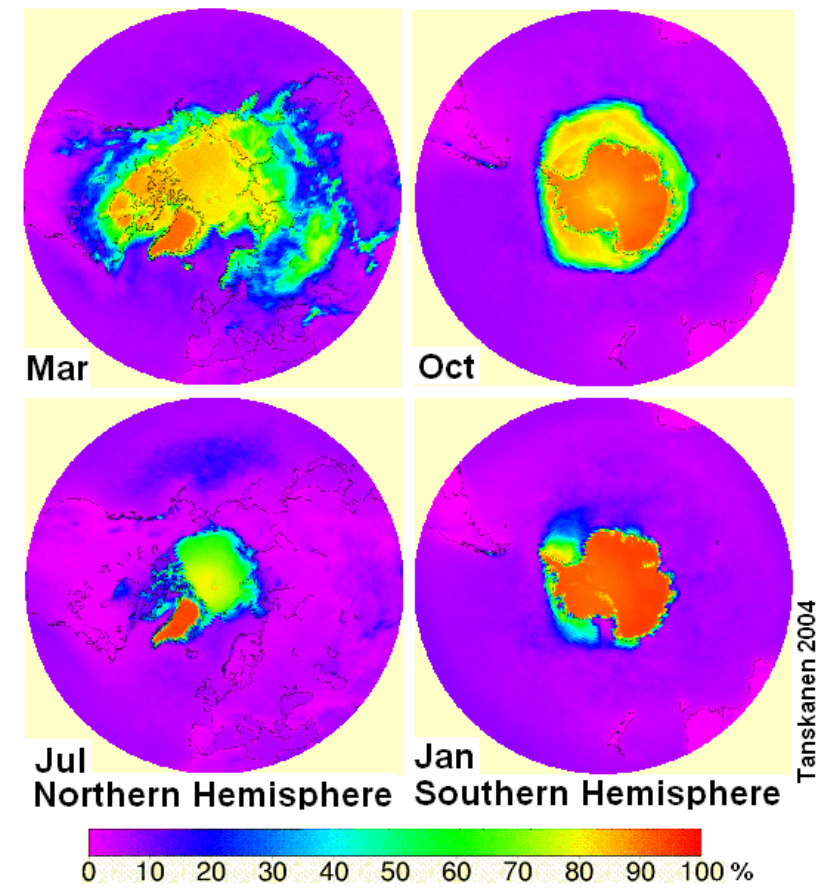

Figure 9 Lambertian surface albedo climatology, MTW algorithm applied on TOMS at 360 nm, months with highest variability in the seasonal cycle (Tanskanen 2004, ttp://promote.fmi.fi/MTW_www/MTW.html).

The regional albedo is forecasted according to Schwander et al. (1999) and Lapeta et al. (2001) using the predicted water content of snow cover. The resulting deviations between modelled and measured UV irrandiance for the snow conditions are *not* significantly higher than for snow free conditions (Schwander et al. 1999).

The increase of the UV Index resulting from adjustment to snow and ice albedo can be seen in Fig. 2e against Fig. 2d only over Greenland and the arctic sea ice since it is an example for northern hemisphere summer conditions. After adjustment of the large-scale UV Index to AOD and altitude this step of adjustment to albedo results in the UV Index for clear sky.

4.4. Adjusting for cloudiness

Besides the solar zenith angle and the total ozone column, clouds are the most important factor affecting UV radiation reaching the ground. Cloud droplet can be assumed as almost purely scattering media. Since the size of the droplets is large compared to the UV wavelengths the spectral behaviour of cloud extinction is not well pronounced and their phase function is characterised by a strong forward scattering peak. The most challenging problem is the high micro- and macro-physical variability of clouds, both, with respect to space and to time (Koepke et al. 2002). The effect of clouds on UV irradiance at the ground is expressed by the ratio between UV irrandiance under cloudy conditions and that for the same atmospheric conditions but for clear sky (Cloud Modification Factor, CMF). Overcast conditions always reduce UV irradiance at the ground. Due to the distinct difference in the diffuse component the relation between radiation reduction by

clouds in the visible and in the UV is non-linear and depends additionally on the SZA. The height of the cloud base is of minor importance for UV irradiance.

Fig. 10 compares modelled CMF's against "true" CMF's based on different neural networks (Schwander et al. 2002) trained with measurements at one alpine site in Germany. The quality of the correlation depends strongly on the input available for modelling. The bottom quality is achieved by applying exclusively the total cloud cover (Fig. 10 a). Information on the cloud cover separated for the ceilings low, medium high, and high (Fig. 10 b) leads to a great improvement. Further refinement is possible by providing additional information whether the solar disk is obscured by clouds or not (Fig. 10c). Best results are achieved using total cloud cover and global irradiation as input (Fig. 10d).

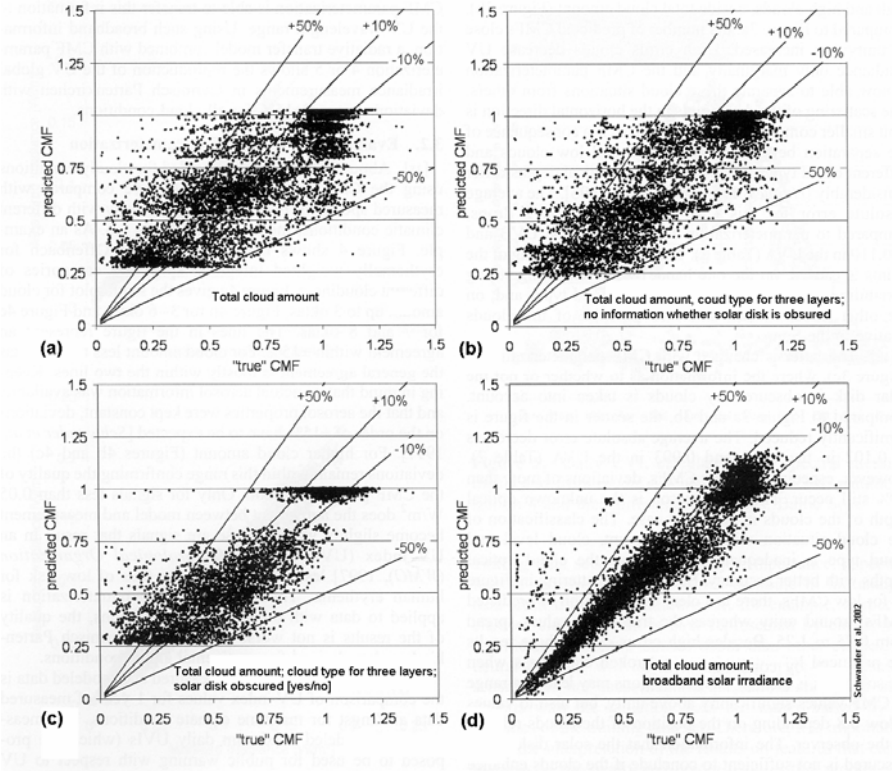

Figure 10 Scatter-plot between true and modelled cloud modification factors (CMF) [source: Schwander et al. 2002]. Required input of the neural networks: (a) total cloud cover, (b) cloud cover in the ceilings low, medium, high, (c) as (b) plus information, solar disk obscured by clouds [y/n], (d) total cloud cover and total short wave irradiance.

Current DWD operationally applies CMF's consisting of 6 classes depending on forecasted cloud cover in the three ceilings low, medium high, and high. (Staiger et al. 1998), and are recommended by COST-713 (Vanicek et al. 2000). The lowest CMF belonging to the forecasted cloud cover in the three levels is used for the adjustment of the UV Index. The CMF's vary between 1 for clear sky and about 0.2 for sky overcast with low clouds that are optically thick. The resulting UV Index for all effective atmospheric conditions including clouds is shown in Fig. 2f, that points up the decisive influence of clouds on the UV Index.

5. Product examples

The forecasts have a resolution in time of one hour allowing a reassembly of the hourly values to the daily maximum of UV Index and the accumulation to the daily erythemal effective UV dose. Selected is an example of the 2004 Antarctic ozone hole, Fig. 11. Due to the decreasing solar zenith angle at local noon for the end of October there are distinct UV effects of the ozone hole. They are amplified by the altitude of the Antarctic plateau of about 3000 m and by the albedo effects of snow and ice, in particular by sea ice having

its broadest expansion in the seasonal cycle. However, the daily maximum of UV Index for all atmospheric conditions demonstrates that this effect can be widely masked by clouds very frequent in this region.

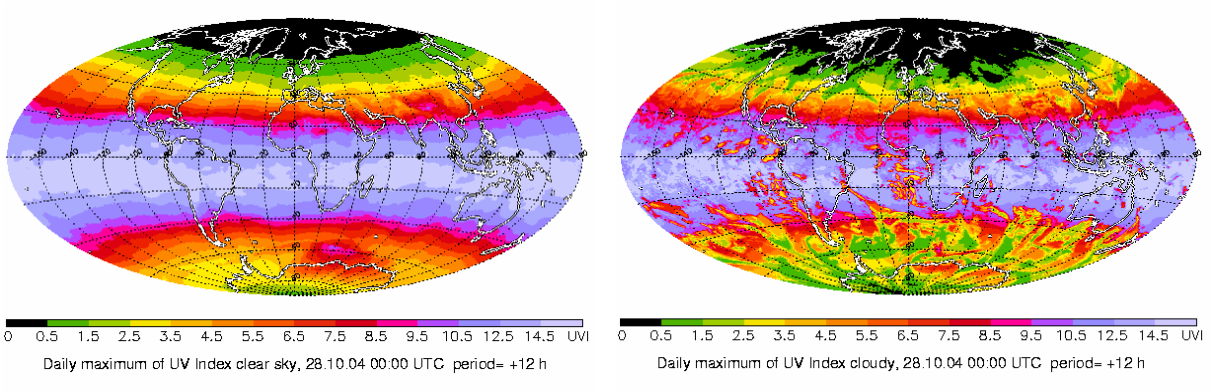

(a) ***(b)***

Figure 11 Antarctic ozone hole and daily maximum of UV Index, 28.10.2004: (a) clear sky, (b) inclusive cloud effects

6. Verifications

Verifications include the forecasts of total column ozone as well as the UV Index. A continuous verification of the forecasts of total column ozone is done on a monthly basis. The applied ozone forecast reassembled according to the satellite overpass times is validated versus TOMS measurement. The root mean square errors vary globally between 3 and 5 %. In moderate and high latitudes the variance can be reduced by more than 70 % compared to forecast of persistence. Thus, the ozone forecasts are essential. In the tropics and in parts of the subtropics too the total column ozone is almost unchanged from day to day. Hence, there is no forecast skill.

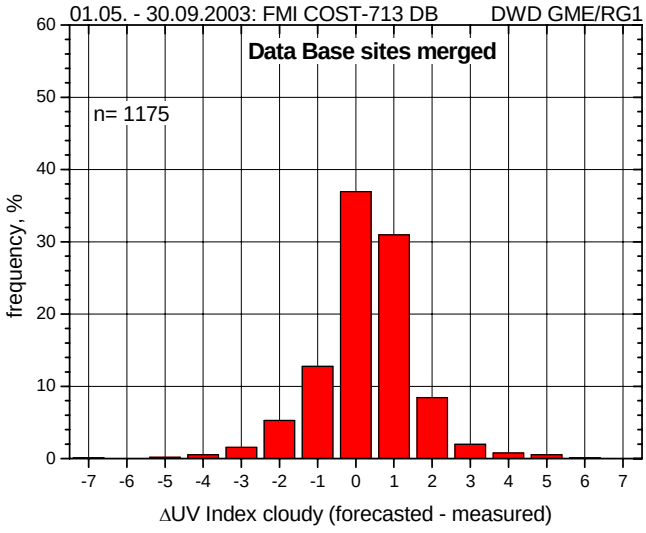

Figure 12 Comparison between forecasted daily maximum of UV Index cloudy and measurements of 11 sites over Europe, May to September 2003

The largest uncertainty in UV-Index forecast is accounted for cloud modification. The forecasted UV Index have been compared to measured values available for 14 European locations between 60° and 43° N for 1999 within the framework of COST-713 (Koepke et al. 2001) and for 11 European stations between 67° and 32° N for May to September 2003. The comparison between the years 1999 and 2003 is assumed to reflect the effect of the improved algorithms used in 2003. The measured data were stored at the COST-713 UV Index data base hosted by the Finnish Meteorological Institute. The daily maximum of the UV Index was retrieved from the measurements of a location and compared to the forecasted UV Index taking into account all effective atmospheric conditions of the next clock hour. In 1999 the forecast of the total column ozone was on a lower quality level, the AOD was fixed (0.2) and the altitude effect was not taken into account. Nevertheless, if the total column ozone was adapted to the measured values, the agreement between forecasted and measured UV Index was in the range of ±1 UV for

more than 56 % of the days, except the mountain stations Hoher Sonnblick and Zakopane. Reduced to cloud free conditions forecasted and measured UV Index agreed within ±1 for nearly 90 % of the days. For 2003, with the improved algorithms, for 80 % of the days the forecasted UV Index for all weather conditions are in the range of ±1 UV Index of the measurement. There are significant differences in the bias between the sites depending on locally enhanced or lowered aerosol properties compared to the climatological values used in forecasting. First comparisons with the TOMS erythemal UV product for satellite overpass times show that the root mean square error is comparable to that of cloud forecasts compared to observed cloudiness.

7. Outlook

In extreme cases aerosols can influence the UV Index up to an amount comparable to that of day to day changes in total ozone column (Jaroslawski and Krzyscin 2005). UV Index forecasting is prepared to include current values of aerosol properties as aerosol optical depth and aerosol type. The “Global Earth Monitoring System (GEMS)” could become a source providing operationally and near real time such data, gridded by data assimilation techniques and having global coverage. Hence, in future such fields of forecasted data should be available.

The largest uncertainty in UV forecast is due to the present cloudiness, which is not a surprise since for the maximum UV Index not only the presence of clouds, but also their time of appearance, their optical depth and their modification of the irradiance as effect of broken cloudiness has to be forecasted. With respect to this point improvements in the future will be possible. COST-Action 726 on “UV climatology and UV trends” evaluates such methods. Its results shall enable to select appropriate algorithms to improve forecasting in respect to cloudiness.

Acknowledgements

The development of the forecast methods was supported by the European Commission through the COST Action 713 and the STREAMER project (FP4: CT97-0756, DG XII). The MODIS MOD08_M3 data came from the NASA Goddard Space Flight Centre (http://modis-atmos.gsfc.nasa.gov/MOD08_M3/index.html). Our sincere thanks go to Dr. Stefan Kinne, Max Planck Institute for Meteorology, and via him to Dr. Omar Torres, NASA Goddard Space Flight Center, for the monthly mean of the aerosol optical depth derived from TOMS. We also owe thanks to the Finnish Meteorological Institute for access to the UV Index database and to the contributors to that database which provided the measurements for comparisons. We would like to thank the Royal Netherlands Meteorological Institute providing the GSE PROMOTE ozone forecasts. Special thanks go to the Meteorological Institute of the University of Munich for their expert advice in radiation transfer calculations, and the many tools valuable in operational forecasting.

5. References

Arola, A., J. Kaurola, L. Koskinen, A. Tanskanen, T. Tikkanen, P. Taala, J.R. Herman, N. Krotkov, V. Fioletov (2003): A new approach to estimating the albedo of snow-covered surfaces in the satellite UV method. *J. Geophys. Res*. **108**, No. D17: ACL 2-1 – 2-5, doi: 10.1029/2003JD003492.

Bais, A.F. (1999): "UV-B Forecasting (COST Action on Meteorology)", *presented at the Weather, Climate and Health Symposium, Lisbon*, 23 March 1999.

Bittner, M., T. Erbertseder (2000): The STREAMER Project: An Overview – in: Longhurst, J.W.S., C.A. Brebbia, H. Power (eds.): *Air Pollution VIII*, S. 473-482, WIT Press, Southhampton, Boston.

Blumthaler, M. W. Ambach (1988): Solar UVB albedo of various surfaces. *Photochem. Photobiol.* **48**: 85-88.

Blumthaler, M., W. Ambach, M. Huber (1993): Altitude effect of solar UV radiation dependent on albedo, turbidity, and solar elevation. *Meteor. Z.*, N.F. **2**, 116-120.

CIE (1987): A reference action spectrum for ultraviolet induced erythema in human skin. CIE Research Note. *CIE Journal* **6**, 17-22.

De Backer, H., P. Koepke, A. Bais, X. de Cabo, T. Frei, D. Gillotay, C. Haite, A. Heikkilä, A. Kazantzidis, T. Koskela, E. Kyrö, B. Lapeta, J. Lorente, K. Masson, B. Mayer, H. Plets, A. Redondas, A. Renaud, G. Schauberger, A. Schmalwieser, H. Schwander, K. Vanicek (2001): Comparison of Measured and Modelled UV Indices for the Assessment of Health Risks. *Meteorol. Appl.* **8**: 267-277.

Dethof, A., E.V. Hólm (2004a): Representation of ozone in the ECMWF model. *Proceedings of the ECMWF/SPARC Workshop on Modelling and Assimilation for the Stratosphere and Tropopause*, 23 to 26 June 2003, Reading, pp. 107 – 116.

Dethof, A., E.V. Hólm (2004b): Ozone assimilation in the ERA-40 reanalysis project. *Q. J. R. Meteorol.* **130**, 2851-2872.

Eskes, H.J., P.F.J. van Velthoven, H.M. Kelder (2002): Global ozone forecasting based on ERS-2 GOME observations, *Atmos. Chem. Phys*., **2**, 271-278.

Feister, U., R. Grewe (1995): Spectral albedo measurements in the UV and visible region over different types of surfaces. *Photochem. Photobiol.,*. **62**, No.4, 736 –744.

Grenfell; T. C., S. G. Warren, P. C. Mullen (1994): Reflection of solar radiation by the Antarctic snow surface at ultraviolet, visible, and near-infrared wavelengths. *J. Geophys. Res.* **99**, No. D9, 18669 – 18684.

ICNIRP (1995): Global Solar UV Index. A joint recommendation of the World Health Organization, the World Meteorological Organization, the United Nations Environment Programme, and the International Commission on Non-Ionizing Radiation Protection. Oberschleißheim. ISBN 3-9804789-0-4.

Hess, M., P. Koepke, I. Schult (1998): Optical Properties of Aerosol and Clouds: The software package OPAC. *Bull. Am. Met. Soc*. **79**, No.5, 831-844.

Jaroslawski J.P., J.W. Krzyscin (2005): Importance of aerosol variations for surface UV-B level: Analysis of ground-based data taken at Belsk, Poland, 1992–2004. *J. Geophys. Res.* **110**, D16201, doi: 10.1029/2005JD005951.

Kaufman ,Y.J., D. Tanré, O. Boucher (2002): A satellite view of aerosols in the climate system. *Nature* **419**, 215-223.

Koepke, P., M. Hess, I. Schult, E.P. Shettle (1997): Global Aerosol Data Set. *Max-Planck-Institut für Meteorologie, Report* No. 243, pp. 44.

Koepke, P., A.F. Bais, D. Balis, M. Buchwitz, H. de Backer, X. de Cabo, P. Eckert, P. Eriksen, D. Gillotay, T. Koskela, V. Lapeta, Z. Litynska, J. Lorente, B. Mayer, A. Renauld, A. Ruggaber, G. Schauberger, G. Seckmeyer, P. Seifert, A. Schmalwieser, H. Schwander, K. Vanicek, M. Weber (1998): Comparison of Models used for UV Index Calculations. *Photochem. Photobiol*. **67**, 657-662.

Koepke, P., H. De Backer, P. Eriksen, U. Feister, D. Grifoni, T. Koskela, A. Lehmann, Z. Litynska, A. Schmalwieser, H. Staiger, K. Vanicek (2001): An overview of the results from the comparison of UV-Index forecasted and measured at all atmospheric conditions including clouds, in *IRS 2000: Current Problems on Atmospheric Radiation*, Deepack Publ. Hampton Virginia, pp. 1181 – 1184.

Koepke, P., J. Reuder, H. Schwander (2002): Solar UV radiation and its variability due to the atmospheric components. *Recent Res. Devel. Photochem. Photobiol*. **6**, 11-34.

Lapeta, B., H. Schwander, P. Koepke (2001): Adaption of Radiative Transfer Modelling to Simulate UV Radiation on Top of a Mountain, in *IRS 2000: Current Problems on Atmospheric Radiation*, Deepack Publ. Hampton Virginia, pp. 373-376.

Labitzke, K., J.J. Barnett, and B. Edwards (eds.) (1985): *Middle Atmosphere Program*, MAP Handbook, Volume 16, University of Illinois, Urbana.

Li, D., K.P. Shine (1995): The UGAMP ozone climatology and associated software. Department of Meteorology, University of Reading.
http://www.badc.rl.ac.uk/data/ugamp-o3-climatology/ugamp_help.html.

Lim, H.W., B.A. Gilchrest, K.D. Cooper, H.A. Bischoff-Ferrari, D.S. Rigel, W.H. Cyr, S. Miller, V.A. DeLeo, T.K. Lee, C.A. Demko, M.A. Weinstock, A. Young, L.S. Edwards, T.M. Johnson, S.P. Stone (2005): Sunlight, tanning booths, and vitamin D. Conference of the American Academy of Dermatology, organizer H.W. Lim. *J Am Acad Dermatol* **52**, 868-876.

Madronich, S., R.L. McKenzie, L.O. Björn, M.M. Caldwell (1998): Changes in biologically active ultraviolet radiation reaching the Earth's surface. Photochem. Photobiol. **46**: 5-19.

Majewski, D., D. Liermann, P. Prohl, B. Ritter, M. Buchhold, T. Hanisch, G. Paul, W. Wergen, J. Baumgardner (2002): The Operational Global Icosahedral-Hexagonal Gridpoint Model GME: Description and High-Resolution Tests. *Monthly Weather Review* **130**, 319-338.

McClatchey, R.A., R.W. Fenn, J.E.A. Selby, F.E. Volz, J.S. Garing (1972): Optical Properties of the Atmosphere (Third Edition). Air Force Cambridge Research Laboratories. AFCRL-72-0497, *Environ. Res. Papers,* No. 411.

Mech M., P. Koepke (2004): Model for UV irradiance on arbitrarily oriented surfaces, *Theor. Appl. Climatology* **77**, 151-158.

McKenzie, R.L., P.V. Johnston, D. Smale (2001): Altitude effects on UV spectral irradiance deduced from measurements at Lauder, New Zealand, and at Mauna Loa Observatory, Hawaii. *J. Geophys. Res*. **106** D19, 22,845-22,860.

Peuch, V.-H., M.-L. Cathala, O. Dessens, B. Josse, P. Simon, A. Peuch, J. Pailleux, J.-P. Cammas (2004): Simulations and forecasts in the UTLS and stratosphere with the chemistry and transport model MOCAGE *Proceedings of the ECMWF/SOARC Workshop on Modelling and Assimilation for the Stratosphere and Tropopause*, 23 to 26 June 2003, Reading, pp. 155 - 168.

Piazena, H. (1996): The effect of altitude upon the solar UV-B and UV-A irradiance in the tropical Chilean Andes. *Solar Energy* **57,** 133 - 140.

Pfeifer, M. (2003): *Abhängigkeit der UV-Strahlung von der Seehöhe: Untersuchung am Beispiel Bolivien*. Diploma Thesis, Fakultät für Physik der Ludwig-Maximilians-Universität München, pp. 97.

Press, W.H., S.A. Teukolsky, W.T. Vetterling, B.P. Flannery (1996): *Numerical Recipes in Fortran 77*. 2. Edition, Cambridge University Press. New York.

Rees D, J.J. Barnett, K. Labitzke (ed.) (1990): COSPAR International Reference Atmosphere: 1986, Part II: Middle Atmosphere Models. *Advances in Space Research,* Vol. **10** No. 12. Pergamon Press.

Reuder, J., H. Schwander (1999): Aerosol effects on UV radiation in nonurban regions. J. Geophys. Res. **104**, No. D4, 4065-4077.

Ruggaber, A., R. Dlugi, T. Nakajima (1994): Modelling radiation quantities and photolysis frequencies in the troposphere. *J. Atmos. Chem*. **18**, 171-210.

Schmucki, D., R. Philipona (2002): Ultraviolet radiation in the Alps: The altitude effect. *Opt. Eng*. **41** (129), 3090 – 3095.

Schwander, H., P. Koepke, A. Ruggaber (1997): Uncertainties in modeled UV irradiance due to limited accuracy and availability of input data. *J. Geophys. Res*. **102**, No. D8, 9419-9429.

Schwander, H., B. Mayer, A. Ruggaber, A. Albold, G. Seckmeyer, P. Koepke (1999): Method to determine snow albedo values in the ultraviolet for radiative transfer modeling. *Appl. Optics* **38**, 3869-3875.

Schwander, H., A. Kaifel, A. Ruggaber, P. Koepke (2001): Spectral radiative-transfer modeling with minimized computation time by use of a neural-network technique. *Appl. Optics* **40**, 331-335.

Schwander; H., P. Koepke, A. Kaifel, G. Seckmeyer (2002): Modification of spectral UV irradiance by clouds. *J. Geophys. Res*. **107**, No. D16 AAC 7-1 to AAC 7-12.

Staiger, H., P. Koepke (2005): UV Index forecasting on a global scale. *Meteorol. Z.* Vol 14 No. 2, 259-270.

Staiger, H., G. Vogel, U. Schubert, R. Kirchner, G. Lux, G. Jendritzky (1998): UV Index Calculation by the Deutscher Wetterdienst and Dissemination of UV Index Products, in WMO (1998): Report on the WMO-WHO Meeting of Experts on Standardization of UV Indices and their Dissemination to the Public, WMO/TD-No. 921, pp. 89-92.

Tanskanen, A: (2004): Lambertian Surface Albedo Climatology at 360 nm from TOMS Data Using Moving Time-Window Technique. In: *Proceedings XX. Quadrennial Ozone Symposium,* 1-8 June 2004, Kos, Greece.

Torres, O., P.K. Bhartia, J.R. Herman, A. Sinyuk, P. Ginoux, B. Holbein (2002): A Long-Term Record of Aerosol Optical Depth from TOMS Observations and Comparison to AERONET Measurements. *J Atmos. Sciences* **59**, 398-413.

Vanicek, K., T. Frei, Z. Litynska, A. Schmalwieser (2000): UV-Index for the Public. A guide for publication and interpretation of solar UV Index forecasts for the public prepared by the Working Group 4 of the COST-713 Action “UVB Forecasting". COST-713 Action, European Commission, Luxembourg: Office for Official Publications of the European Communities, pp. 27.

WHO (2002): Global solar UV index: a practical guide. A joint recommendation of the World Health Organization, World Meteorological Organization, United Nations Environmental Programme, and the International Commission on Non-Ionizing Radiation Protection. World Health Organization, Geneva. ISBN 92 4 159007 6.

WHO (2003): INTERSUN, The Global UV Project. A Guide and Compendium. Radiation and Environmental Health Unit, Protection of the Human Environment. World Health Organization, Geneva.

WMO (1995): Report on the WMO Meeting on Experts on UV-B Measurements, Data Quality and Standardization of UV Indices (Les Diablerets, 25-28 July, 1994). GAW, Report No. 95, Geneva.

WMO (1998): Report on the WMO-WHO Meeting of Experts on Standardization of UV Indices and their Dissemination to the Public, Les Diablerets, Switzerland, WMO/TD-No. 921.

Annex: Seasonal Variations in Aerosol Optical Depths and Aerosol types

A1. Introduction

To improve the aerosol effect in the large-scale UV Index it would be advantageous to use current values of the aerosol optical depth at 550 nm (AOD) instead of the standard 0.2, but forecasted values of AOD are not yet available. However, a strong improvement already can be made by using regional values of AOD with seasonal variations on a monthly basis. Such values have been derived from the MODIS (**Mod**erate Resolution **I**maging **S**pectroradiometer) sensors (Kaufman et al. 2002) of the NASA "Earth Observing Systems (EOS)". The algorithms of the remote sensing of tropospheric aerosols by MODIS are described by Kaufman and Tanré (1998). Martins et al. (2002) report on the method for identifying cloud-free pathways, Ichoku et al. (2002) on the spatio-temporal approach for global validation and analysis of MODIS aerosol products. Remer et al. (2002) validated MODIS aerosol retrieval over oceans, and Chu et al. (2002) over land. The NASA Goddard Space Flight Center compiles monthly global values of gridded data from these products (MOD08_M3). The grid has a resolution of 1 degree in latitude and longitude.

The monthly AOD distributions over oceans and land agree well with ground- and earlier satellite-based measurements and basically also with model calculations (Penner et al. 2002, Li and Ramathan 2002, Ramachandran and Jayaraman 2003, Pinker et al. 1997, Husar et al. 1997, Smirnov et al. 1995). In the monthly charts an increased variability in the boundary regions of the moderate latitudes in relation to the polar latitudes is noticeable and in agreement with other studies (Myhre et al. 2004). In the transition to the polar areas without data large areas with aerosol optical depths > 0.9 appear over the north Pacific and the north Atlantic, especially in the months of April and May, and partly enhanced values in the mid-latitude southern oceans too. In these areas it is highly probable that the sky is cloudy and there is fog and mist in the cold water areas. Even in the cloud-free pathways a subpixel cloud, snow/ice, and water contamination cannot be completely ruled out (Chu et al. 2002, Remer et al. 2002). This leads to higher values and a higher degree of scattering around the mean values, interpreted as high AOD. The cloud fraction effect could result in a 10 – 20 % overestimation in monthly mean aerosol optical depth (Zhang et al. 2005). In the following it is described, how such effects are reduced, and how the missing data areas in MODIS are closed.

A2. Reduction of enhanced spatial variability in AOD

There are still few months available with MODIS MOD08_M3 data. The increased spatial variability found in parts can thus not yet be equated by a sufficiently high number of months for a "climatology" of the aerosol optical depths. The aim is an algorithm that reduces the variability of the AOD. However it has to be pointed out that the AOD’s are used as input parameters for UV Index determination. Thus, to stay on the safe side, in case of doubt the algorithm should lead to a forecasted UV Index that is too high rather than too low, i.e. the derived AOD should be low.

The monthly charts, Fig. 1a, show that high spatial variability of the AOD’s is to be expected in those areas where the number of the available "pixel counts" for the calculation of the monthly mean in the 1°·1° field is small. They are subject to large fluctuations. The data of a month were sorted according to pixel counts and divided into a class width of 5 %. It can be followed from a low pixel count that a large number of measurement points with clouds existed during the month. Thus, the probability of a sub-pixel cloud contamination increases for the remaining pixels classed as cloud-free. The mean AOD will be raised because clouds are always bright. For this reason the value of the monthly mean is

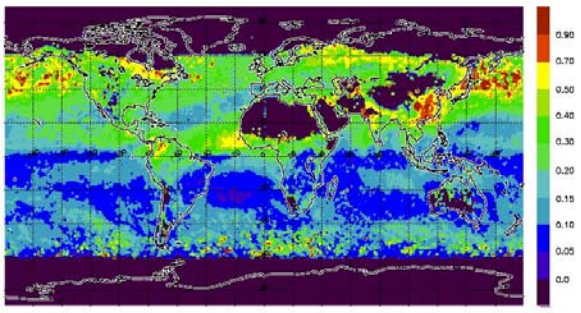

Fig. 1a: April 2001: NASA MOD08_M3 Optical_ Depth_Land_And_Ocean_Mean_Mean; unchanged..

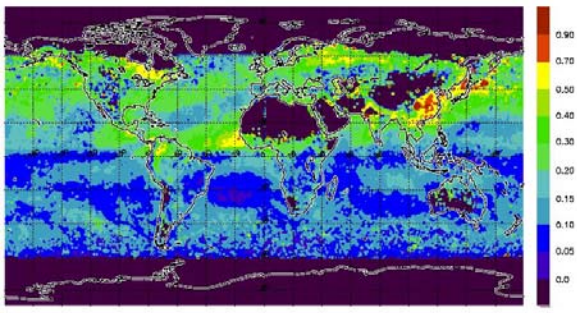

Fig. 1b: April 2001: NASA MOD08_M3 Optical_ Depth_Land_And_Ocean_Mean_Mean; condition after reduction.

to be reduced. To a certain extent similar to the procedure of Zhao et al. (2003), the monthly means of the AOD are reduced when their pixel count sinks below the 50 percentile. The difference of the pixel counts 50 percentile minus 15 percentile value is formed, i.e. the scaling value. A weighting factor is calculated from the pixel count for a measured value minus pixel count of the 50 percentile divided by the scaling value. The weighting factor grows with decreasing percentile values of the pixel count, thus taking into account the increasing variance of the standard deviation around the class mean. A monthly mean of the AOD of a grid point is then reduced under the condition that this AOD is larger than the mean values minus 0.5 standard deviation of the percentile class which belongs to the single value. The reduced value of this grid point is then, measured monthly mean of the AOD minus measured standard deviation, multiplied by the weighting factor. If this reduced value is smaller than the measured minimum, then the measured minimum is used. From Fig. 1b it can be seen spatially that the large changes are concentrated on the boundary areas of the polar regions, and that small changes also occur in areas frequently covered in thick cloud, e.g. in the inter-tropical convergence zone or the middle to near-polar regions of the moderate latitudes.

A3. Treatment of missing data areas in MODIS

The great deserts show only missing data in MODIS. Provided that no aerosol optical depths are available from MODIS, the gaps are closed by derivations of the aerosol optical depth from the NASA Total Ozone Mapping Spectrometer (TOMS) as extensive data of the next best quality, Fig. 2. New algorithms for the derivation of aerosol properties were used on the TOMS data for the years 1979 to 2001 (Torres et al. 2002, Prospero et al. 2002). The assumption of the important aerosol altitude for dust within these algorithms is based on the model of Ginoux et al. (2001) for determining the AOD from TOMS.

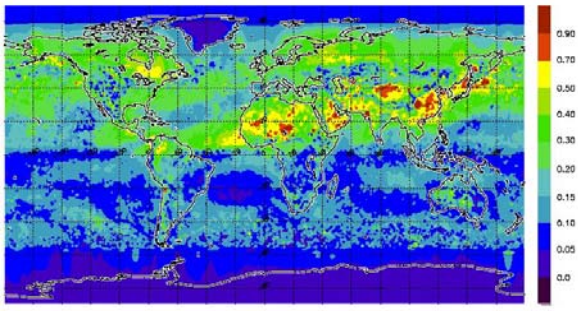

Fig. 2: April 2001: NASA MOD08_M3 Optical_ Depth_Land_And_Ocean_Mean_Mean; conditions after reduction and introduction of TOMS monthly means and set values of the pole caps.

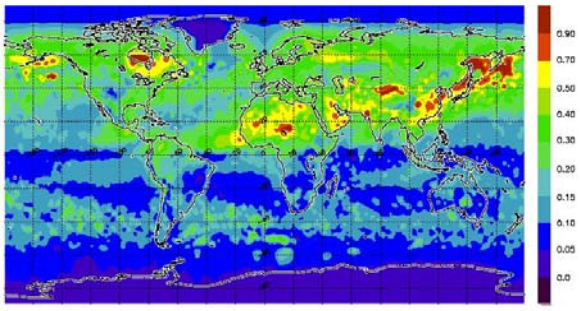

Fig. 3: April, average 2000 – 2003 of pre-processed NASA MOD08_M3 Optical_Depth_Land_And_ Ocean_Mean_Mean

The pole caps show also missing data in MODIS and TOMS. In order to fill these areas with an AOD, a background value of the aerosol optical depth is set in parts of the polar regions. Smirnov et al. (1995) measure minimal values of 0.06 in the arctic air masses of the north Atlantic. Koepke et al. (1997) use 0.05 as background value in the "Global Aerosol Data Set". Herber et al. (2002) found in the autumn on Spitsbergen (1991-1999) a mean seasonal minimum aerosol optical depth of 0.031 which they refer to as background value, and a spring maximum of 0.089 due to "arctic haze". In Tasmania Wilson and Forgan (2002) measure in the period 1986 - 1999 an aerosol optical depth of 0.04 at 500 nm in the annual mean with minima in winter of 0.01. The data apply to inshore winds and are reduced by the influence of the Mount Pinatubo eruption. They are thus representative of large parts of the southern oceans. In the AOD algorithm in the polar regions an AOD of 0.031 is set as general background value for latitudes higher than 85° and for sea level. The AOD is reduced additionally, depending on the altitude profile of the aerosol for the entire Antarctic plateau above 500 m. This gives a background value of the AOD of 0.01 at altitudes of around 3000 m and results in a comparatively sharp gradient in the interpolation from the ice edge to the first measured values towards the equator. The same procedure is also used for the inland ice on Greenland. In the Arctic the annual variation of the aerosol optical depth is to be taken into consideration (Barrie 1986, Koepke et al. 1997). It is parameterised from the measurements from Herber et al. (2002) by two parabolas between maximum and minimum. This annual variation is set for all latitudes higher than 80° N, independent of the fact that, according to Barrie (1986) the Eurasian part of the Arctic is increasingly being affected by "arctic haze". Between the edge of the polar background value linear interpolation is carried out along each degree of longitude up to the first measured value. This measured value is replaced by a value which results from the overlapping averaging of measured value and the 5 next measured values towards the equator. Each value of the pole caps thus set is subsequently smoothed by overlapping averaging of the ±5 next values of varying longitude but fixed latitude.

The few remaining mutual missing MODIS and TOMS points are interpolated from the surrounding values. The interpolation is by $1/r^2$ from the next 4 points on each point of the compass that shows values. Fields of the same months are averaged arithmetically. As the MODIS series are still short, a conclusive light smoothing is carried out with the surrounding points by means of a weighted mean. Fig. 3 shows the resulting global AOD distribution for April as an example.

For the Indian Ocean Li and Ramathan (2002) show, with five years of satellite measurements by NOAA-AVHRR, that the variability between individual years can be very different spatially. Thus the monthly mean AOD, of course, may change in the future if longer series of well calibrated measurements can be used. However at the moment, the AOD data set is a very good basis for the global UV Index modelling.

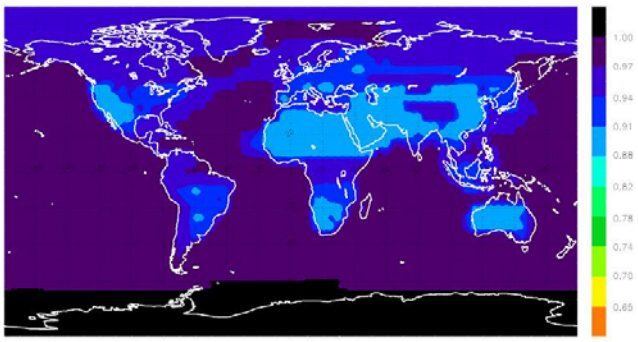

Fig. 4: Single scattering albedo at 300 nm (SSA), calculated for a relative humidity of 70 % and limited to SSA > 0.887: Summer (Koepke et al. 1997)

A4. Single Scattering Albedo

A global distribution of the single scattering albedo at 300 nm (SSA) of the tropospheric aerosol is not available from satellite data. For this quantity values have been derived for summer and winter from the "Global Aerosol Data Set" (Koepke et al. 1997) in a grid of 5°·5° using a relative humidity of 70 %, Fig. 4. Values lower than the SSA of the aerosol type "continental average" are limited to the SSA of

that aerosol type. In the Atlantic area off the North-African west coast it is additionally accounted for westward driven Saharan dust.

Acknowledgements

The MODIS MOD08_M3 data came from the NASA Goddard Space Flight Centre (http://modis-atmos.gsfc. nasa.gov/MOD08_M3/index.html). Our sincere thanks go to Dr. Stefan Kinne, Max Planck Institute for Meteorology, and via him to Dr. Omar Torres, NASA Goddard Space Flight Center, for the monthly mean of the aerosol optical depth derived from TOMS. The Global Aerosol Data Set has been provided by the University of Munich via http://www.lrz-muenchen.de/~uh234an/www/radaer/gads.html.

References:

Barrie, L.A. (1986): Arctic Air Pollution: An Overview of Current Knowledge. *Atmospheric Environment* **20,** 643-663.

Chu, D.A., Y.J. Kaufman, C. Ichoku, L.A. Remer, D. Tanré, B.N. Holben (2002): Validation of MODIS aerosol optical depth retrieval over land. *Geophysical Research Letters* **20**, MOD 2-1, 2-4.

Ginoux, P., M. Chin, I. Tegen, J.M. Prospero, B. Holben, O. Dubovik; S-J. Lin (2001): Sources and distributions of dust aerosols simulated with the GOCART model. *J. Geophys. Res*. **106**, No. D17, 20,255-20,274.

Herber, A., L.W. Thomasson, H. Gernandt, U. Leiterer, D. Nagel, K-H. Schulz, J. Kaptur, T. Albrecht, J. Notholt (2002): Continuous day and night aerosol optical depth observations in the Arctic between 1991 and 1999. *J. Geophys. Res.* **107**, No. D10, AAC 6-1 - 6-13.

Husar, R.B., J.M. Prospero, L.L. Stowe (1997): Characterization of tropospheric aerosol over the oceans with the NOAA advanced very high resolution radiometer optical thickness operational product. *J. Geophys. Res.* **102** D14, 16,889-16,909.

Ichoku, C., D.A. Chu, S. Mattoo, Y.J. Kaufman, L.A. Remer, D. Tanré, I. Slutsker, B.N. Holben (2002): A spatio-temporal approach for global validation and analysis of MODIS aerosol products. *Geophysical Research Letters* **20**, MOD 1-1, 1-4.

Kaufman, Y.J., D. Tanré (1998): Algorithm for remote sensing of tropospheric aerosol from MODIS. http://modis-atmos.gsfc.nasa.gov/MOD08_M3/atbd.html. Product ID: MOD04, pp. 85.

Kaufman ,Y.J., D. Tanré, O. Boucher (2002): A satellite view of aerosols in the climate system. *Nature* **419**, 215-223.

Koepke, P., M. Hess, I. Schult, E.P. Shettle (1997): Global Aerosol Data Set. *Max-Planck-Institut für Meteorologie, Report* No. 243, pp. 44.

Li, F., V. Ramanathan (2002): Winter to summer monsoon variation of aerosol optical depth over the tropical Indian Ocean. *J. Geophys. Res.* **107**, D16, AAC 2-1, 2-13.

Martins, J.V., D. Tanré, L. Remer, Y. Kaufman, S. Mattoo, R. Levy (2002): MODIS Cloud screening for remote sensing of aerosol over oceans using spatial variability. Validation of MODIS aerosol retrieval over ocean. *Geophysical Research Letters* **20**, MOD 4-1 - 4-4.

Myhre, G., F. Stordal, M. Johnsrud, A. Ignatow, M.I. Mischenko, I.V. Geogdzhayev, D. Tanré, J.L. Deuze, P. Goloub, T. Nakajima, A. Higurashi, O. Torres, B. Holben (2004): Intercomparison of Satellite Retrieved Aerosol Optical Depth over the Ocean. *J. Atmos. Sciences*. **61**, 499-513.

Penner, .JE., S.Y. Zhang, M. Chin, C.C. Chuang, J. Feichter, Y. Fen, I.V. Geogdzhayev, P. Ginoux, P. Herzog, A. Higurashi, D. Koch, C.H. Land, U. Lohmann, M. Mishchenko, T. Nakajima, G. Pitari, B. Soden, I. Tegen, L. Stowe (2002): A Comparison of Model- and Satellite-Derived Aerosol Optical Depth and Reflectivity. *J. Atmos. Sciences*. **59**, 441-460.

Pinker, A.T., R.A. Ferrare, A. Karnieli, T.O. Aro, Y.J. Kaufman, A. Zangvil (1997): Aerosol optical depths in a semiarid region. *J. Geophys. Res*. **102** D10, 11,123-11,137.

Prospero, J.M., P. Ginoux, O. Torres, S.E. Nicholson, T.E. Gill (2002): Environmental Characterization of Global Sources of Atmospheric Soil Dust Identified with the Nimbus 7 Total Ozone Mapping Spectrometer (TOMS) Absorbing Aerosol Product. *Reviews of Geophysics* **1**, 2-1 - 2-31.

Ramachandran, S., A. Jayaraman (2003): Spectral aerosol optical depth over Bay of Bengal and Chennai: II-sources, anthropogenic influence and model estimates. *Atmospheric Environment* **37**, 1951-1962.

Remer, L.A., D. Tanré, Y.J. Kaufman, C. Ichoku, S. Mattoo, R. Levy, D.A. Chu, B. Holben, O. Dubovik, A. Smirnov, J.V. Martins, R-R. Li (2002): Validation of MODIS aerosol retrieval over ocean. *Geophysical Research Letters* **20**, MOD 3-1 – 3-4.

Smirnov, A., Y. Villevalde, N.T. O'Neil, A. Royer, A. Tarussov (1995): Aerosol optical depth over the oceans: Analysis in terms of synoptic air mass types. *J. Geophys. Res*. **100** D8, 16,639-16,650.

Torres, O., P.K. Bhartia, J.R. Herman, A. Sinyuk, P. Ginoux, B. Holbein (2002): A Long-Term Record of Aerosol Optical Depth from TOMS Observations and Comparison to AERONET Measurements. *J Atmos. Sciences* **59**, 398-413.

Wilson ,S.R., B.W. Forgan (2002): Aerosol optical depth at Cape Grim, Tasmania, 1986-1999. *J. Geophys. Res.* **107**, No. D8, AAC 6-1 – 6-9.

Zhang, J., J.R. Reid, B.N. Holben (2005): Analysis of potential cloud artifacts in MODIS over ocean aerosol optical thickness products. *Geophys. Res. Lett.* **32**, L15803, doi_10-1029/2005GL023254.

Zhao, X.-P., I. Laszlo, B.N. Holben, C. Pietras, K.J. Voss (2003): Validation of two-channel VIRS retrievals of aerosol optical thickness over oceans and quantitative evaluation of the impact from potential subpixel cloud contamination and surface wind effect. *J. Geophys. Res.*. **108**, No. D3, AAC 7-1 - 7-12.